

o-Iminobenzosemiquinonato(1–) and *o*-Amidophenolato(2–) Complexes of Palladium(II) and Platinum(II): A Combined Experimental and Density Functional Theoretical Study

Xianru Sun, Hyungphil Chun, Knut Hildenbrand, Eberhard Bothe, Thomas Weyhermüller, Frank Neese, and Karl Wieghardt*

Max-Planck-Institut für Strahlenchemie, Stiftstrasse 34-36,
D-45470 Mülheim an der Ruhr, Germany

Received December 20, 2001

From the reaction mixture of $[M^{II}(\text{bpy})\text{Cl}_2]$, the ligand 2-anilino-4,6-di-*tert*-butylphenol, $\text{H}[\text{L}^{\text{AP}}]$, and 2 equiv of a base (NaOCH_3) in CH_3CN under anaerobic conditions were obtained the blue-green neutral complexes $[M^{II}(\text{L}^{\text{AP}}\text{-H})(\text{bpy})]$ ($M = \text{Pd}$ (**1**), Pt (**2**)). $(\text{L}^{\text{AP}}\text{-H})^{2-}$ represents the *o*-amidophenolato dianion, $(\text{L}^{\text{AP}})^{1-}$ is the *o*-aminophenolato(1–), $(\text{L}^{\text{SQ}})^{1-}$ is its one-electron-oxidized, π -radical *o*-iminobenzosemiquinonato(1–), and $(\text{L}^{\text{BQ}})^0$ is the neutral quinone. Complexes **1** and **2** can be oxidized by ferrocenium hexafluorophosphate, yielding the paramagnetic salts $[M^{II}(\text{L}^{\text{SQ}})(\text{bpy})]\text{PF}_6$ ($S = 1/2$) ($M = \text{Pd}$ (**1a**), Pt (**2a**)). The reaction of PtCl_2 , 2 equiv of $\text{H}[\text{L}^{\text{AP}}]$, and 4 equiv of base in CH_3CN in the presence of air yields diamagnetic $[\text{Pt}(\text{L}^{\text{SQ}})_2]$ (**3**), which is shown to possess an electronic structure that is best described as a singlet diradical. Complexes **1**, **1a**, **2**, **2a**, and **3** have been structurally characterized by X-ray crystallography at 100 K. It is clearly established that O,N-coordinated $(\text{L}^{\text{AP}}\text{-H})^{2-}$ ligands have a distinctly different structure than the corresponding O,N-coordinated $(\text{L}^{\text{SQ}})^{1-}$ radicals. It is therefore possible to unambiguously assign the protonation and oxidation level of *o*-aminophenol derived ligands in coordination compounds. All complexes have been investigated by cyclic voltammetry, spectroelectrochemistry, EPR, and UV–vis spectroscopy. Complexes **1** and **2** can be reversibly oxidized to the $[M^{II}(\text{L}^{\text{SQ}})(\text{bpy})]^+$ and $[M^{II}(\text{L}^{\text{BQ}})(\text{bpy})]^{2+}$ mono- and dications, respectively, and reduced to the $[M(\text{L}^{\text{AP}}\text{-H})(\text{bpy}^*)]^-$ anion, where $(\text{bpy}^*)^{1-}$ is the radical anion of 2,2'-bipyridine. Complex **3** exhibits four reversible one-electron-transfer waves (two oxidations and two reductions) which are all shown to be ligand centered. The EPR spectra of the one-electron-reduced species $[\text{Pt}(\text{L}^{\text{AP}}\text{-H})(\text{L}^{\text{SQ}})]^-$ ($S = 1/2$) and of the one-electron-oxidized species $[\text{Pt}(\text{L}^{\text{SQ}})(\text{L}^{\text{BQ}})]^+$ ($S = 1/2$) in CH_2Cl_2 solutions have been recorded. To gain a better understanding of the electronic structure of **3** and its monooxidized and reduced forms, relativistic DFT calculations have been carried out. Magnetic coupling parameters and hyperfine couplings were calculated and found to be in very good agreement with experiment. It is shown that both the one-electron oxidation and reduction of **3** are ligand centered. A simple MO model is developed in order to understand the EPR properties of the monocation and monoanion of **3**.

Introduction

In a series of papers we have recently established^{1–5} that *o*-aminophenols are redox noninnocent when O,N-coordinated to a transition metal ion Ni(II), Cu(II), Pd(II), Co(III), Fe(III), or Cr(III). We have shown that for example

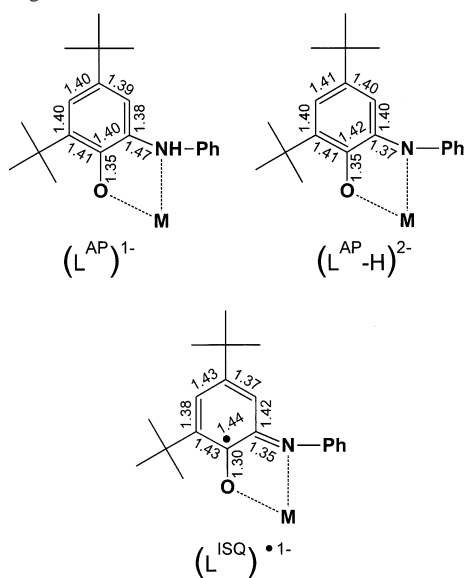
2-anilino-4,6-di-*tert*-butylphenol, $\text{H}[\text{L}^{\text{AP}}]$, can bind to a transition metal ion in an O,N-fashion as (i) diamagnetic *o*-aminophenolato(1–) monoanion, $(\text{L}^{\text{AP}})^{1-}$, or (ii) diamagnetic *o*-amidophenolato(2–) dianion, $(\text{L}^{\text{AP}}\text{-H})^{2-}$, or (iii) paramagnetic ($S_{\text{rad}} = 1/2$) *o*-iminobenzosemiquinonato(1–)

* Author to whom correspondence should be addressed. E-mail: wieghardt@mpi-muelheim.mpg.de.

- (1) Verani, C. N.; Gallert, S.; Bill, E.; Weyhermüller, T.; Wieghardt, K.; Chaudhuri, P. *Chem. Commun.* **1999**, 1747.
- (2) Chaudhuri, P.; Verani, C. N.; Bill, E.; Bothe, E.; Weyhermüller, T.; Wieghardt, K. *J. Am. Chem. Soc.* **2001**, *123*, 2213.

- (3) Chun, H.; Verani, C. N.; Chaudhuri, P.; Bothe, E.; Bill, E.; Weyhermüller, T.; Wieghardt, K. *Inorg. Chem.* **2001**, *40*, 4157.
- (4) Chun, H.; Weyhermüller, T.; Bill, E.; Wieghardt, K. *Angew. Chem., Int. Ed.* **2001**, *40*, 2489.
- (5) Chun, H.; Chaudhuri, P.; Weyhermüller, T.; Wieghardt, K. *Inorg. Chem.* **2002**, *41*, 790.

Scheme 1. Average Bond Distances in (L^{ISQ})^{•-} and O,N-Coordinated (L^{AP-H})²⁻ Ligands^a

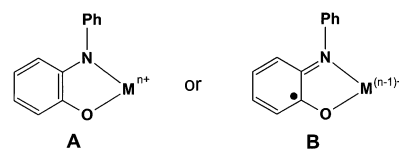


^a From structures in refs 1–5; the estimated error (3σ) is ± 0.01 Å.

monoanion, (L^{ISQ})¹⁻. High-quality, low-temperature X-ray crystallography allows the assignment of protonation and oxidation level of the O,N-coordinated ligand in a given complex. Scheme 1 shows their metrical details. It is noted that no complex containing the neutral quinone form, (L^{IBQ}), has been structurally characterized to date. Complexes containing *o*-aminothiophenolato ligands and their benzo-semiquinonato analogues have also been identified recently.⁶

The square-planar, diamagnetic compounds [M(L^{ISQ})₂] (M = Ni, Pd) and their paramagnetic Cu(II) ($S_i = 1/2$) analogue have recently been described by us.² We have shown that the electronic structure of the Ni and Pd complexes is best described as a species containing a diamagnetic divalent metal ion (d^8) in a square-planar environment of two O,N-coordinated *o*-iminobenzosemiquinonato(1⁻) π -radical ligands. The spins are intramolecularly antiferromagnetically coupled yielding the observed $S = 0$ ground state. Thus these species are singlet diradicals. Here we report the analogous platinum species [Pt(L^{ISQ})₂] ($S_i = 0$) (**3**).

We have also prepared and fully characterized the diamagnetic neutral complexes [M(L^{AP-H})(bpy)] (M = Pd (**1**), Pt (**2**)) which can be reversibly oxidized to the corresponding paramagnetic monocations where bpy represents the neutral ligand 2,2-bipyridine. The following paramagnetic salts have been isolated: [M(L^{ISQ})(bpy)]PF₆ (M = Pd (**1a**), Pt (**2a**)). Complexes **1a** and **2a** are ideally suited to establish the spectroscopic features of a single O,N-coordinated (L^{ISQ})¹⁻ π -radical in a coordination compound. The structures of the pairs **1/1a** and **2/2a** allow the geometrical features of an O,N-coordinated dianion (L^{AP-H})²⁻ versus its one-electron oxidized monoanionic radical (L^{ISQ})¹⁻ to be firmly established. This is of importance when one wishes to discern experimentally between the two forms **A** and **B**.



Experimental Section

The ligand 2-anilino-4,6-di-*tert*-butylphenol, H[L^{AP}],^{1,2} and the complexes [Pd(bpy)Cl₂] and [Pt(bpy)Cl₂]⁷ have been prepared as described in the literature.

[Pd(L^{AP-H})(bpy)] (1). To a solution of the ligand H[L^{AP}] (150 mg; 0.5 mmol) in dry acetonitrile (30 mL) under an Ar blanketing atmosphere was added solid [Pd(bpy)Cl₂] (166 mg; 0.5 mmol) and Na[OCH₃] (0.5 M CH₃OH solution; 2 mL $\hat{=}$ 1.0 mmol). The mixture was heated to reflux for 3 h under Ar. After the solution was cooled to ambient temperature a dark blue crystalline precipitate formed, which was collected by filtration and washed with diethyl ether. Yield: 194 mg (70%). Anal. Calcd for C₃₀H₃₃N₃OPd: C, 64.63; H, 5.92; N, 7.54. Found: C, 64.4; H, 6.0; N, 7.5. ESI mass spectrum: m/z 557 [M⁺] (100%).

[Pd(L^{ISQ})(bpy)]PF₆ (1a). To a deep blue solution of **1** (255 mg; 0.46 mmol) in dry CH₂Cl₂ (50 mL) under an Ar atmosphere was added ferrocenium hexafluorophosphate, [Fc]PF₆ (152 mg; 0.46 mmol). After the solution was stirred at room temperature for 3 h, the solvent was partly removed (\sim 20 mL) by evaporation and *n*-hexane (10 mL) was added. A brown crystalline material formed, which was collected by filtration and washed with diethyl ether. Yield: 287 mg (89%). Anal. Calcd for C₃₀H₃₃N₃OPdPF₆: C, 51.28; H, 4.70; N, 5.98. Found: C, 51.1; H, 4.8; N, 6.0. ESI mass spectrum: m/z 557 [M⁺] (100%).

[Pt(L^{AP-H})(bpy)] (2). To a solution of the ligand H[L^{AP}] (150 mg; 0.5 mmol) in dry acetonitrile (30 mL) under Ar was added solid [Pt(bpy)Cl₂] (179 mg; 0.5 mmol) and Na[OCH₃] (0.5 M CH₃OH solution; 2 mL; 1.0 mmol). After heating to reflux for 3 h, a stream of Ar was passed through the resulting green solution to slowly evaporate the solvent. Within 2 d dark green crystals suitable for X-ray crystallography were obtained. Yield: 210 mg (65%). Anal. Calcd for C₃₀H₃₃N₃OPt: C, 55.73; H, 5.11; N, 6.50. Found: C, 56.0; H, 5.2; N, 6.6. ESI mass spectrum: m/z 646 [M⁺].

[Pt(L^{ISQ})(bpy)]PF₆ (2a). This compound has been prepared as described above for **1a** except that **2** (50 mg; 0.08 mmol) was used as the starting material and an equimolar amount of [Fc]PF₆ (25.6 mg; 0.08 mmol). A red crystalline solid was obtained. Yield: 61 mg (82%). Anal. Calcd for C₃₀H₃₃N₃OPtPF₆: C, 45.51; H, 4.17; N, 5.31. Found: C, 46.0; H, 4.3; N, 5.4. ESI mass spectrum: m/z 646 [M⁺].

[Pt(L^{ISQ})₂] (3). A solution of PtCl₂ (0.30 g; 1.1 mmol), the ligand H[L^{AP}] (0.45 g; 1.5 mmol), and NEt₃ (0.5 mL) in CH₃CN (30 mL) was stirred at 20 °C in the presence of air for 3 h. The dark blue solution was filtered and the solvent was removed by evaporation. The dark blue residue was redissolved in a methanol/acetonitrile mixture (1:1) and the solvent was allowed to slowly evaporate in air. A dark blue microcrystalline powder precipitated. Yield: 0.20 g (34% based on H[L^{AP}]). Single crystals suitable for X-ray diffraction were obtained by recrystallization of dark blue powder from the CH₃CN/CH₂Cl₂ (1:1) mixture. EI mass spectrum: m/z 785 [M⁺]. ¹H NMR (CDCl₃, 400 MHz): δ 7.65 (d, 4H), 7.52 (t, 4H), 7.38 (t, 2H), 6.96 (s, 2H), 6.74 (s, 2H), 1.26 (s, 18H), 1.17 (s, 18H) ppm. Anal. Calcd for C₄₀H₅₀N₂O₂Pt: C, 61.20; H, 6.42; N, 3.57. Found: C, 61.1; H, 6.5; N, 3.6.

(6) Herebian, D.; Bothe, E.; Bill, E.; Weyhermüller, T.; Wieghardt, K. *J. Am. Chem. Soc.* **2001**, *123*, 10012.

(7) Fox, S. G.; Gillard, R. D. *Polyhedron* **1988**, *7*, 349.

Table 1. Crystallographic Data for **1**, **1a**, **2**, **2a**, and **3**

	1	1a	2	2a	3
chem formula	C ₃₀ H ₃₃ N ₃ OPd	C ₃₀ H ₃₃ F ₆ N ₃ OPPd	C ₃₀ H ₃₃ N ₃ OPt	C ₃₀ H ₃₃ F ₆ N ₃ OPPt	C ₄₀ H ₅₀ N ₂ O ₂ Pt
fw	557.99	702.96	646.68	791.65	785.91
space group	P1, no. 2	C2/c, no. 15	P1, no. 2	C2/c, no. 15	P1, no. 2
a, Å	10.1455(9)	26.3425(12)	10.1892(9)	26.296(2)	5.7790(3)
b, Å	11.0851(9)	5.7281(4)	11.2083(9)	5.7372(4)	11.7080(5)
c, Å	13.1358(12)	38.538(2)	13.0067(12)	38.648(3)	13.6868(6)
α, deg	87.15(1)	90	86.83(1)	90	108.51(1)
β, deg	72.93(1)	99.41(1)	72.45(1)	99.38(1)	92.94(1)
γ, deg	64.82(1)	90	65.53(1)	90	94.00(1)
V, Å ³	1273.2(2)	5736.8(6)	1284.9(2)	5752.7(7)	873.37(7)
Z	2	8	2	8	1
T, K	100(2)	100(2)	100(2)	100(2)	100(2)
ρ calcd, g cm ⁻³	1.456	1.628	1.671	1.828	1.494
diffractometer used	Siemens SMART	Nonius Kappa-CCD	Siemens SMART	Nonius Kappa-CCD	Siemens SMART
reflns collected/θ _{max}	14217/33.16	20918/30.00	14304/33.14	18348/30.00	9672/33.17
unique reflns/I > 2σ(I)	8418/6818	8093/6831	8445/7268	7829/6241	5747/5744
no. of params	322	385	322	385	211
μ(Mo Kα), cm ⁻¹	7.57	7.72	54.88	50.03	40.53
R1 ^a /goodness of fit ^b	0.0342/0.953	0.0318/1.054	0.0327/1.006	0.0402/1.011	0.0227/1.054
wR2 ^c (I > 2σ(I))	0.0659	0.0687	0.0657	0.0745	0.0540

^a Observation criterion: $I > 2\sigma(I)$. $R1 = \sum ||F_o| - |F_c|| / \sum |F_o|$. ^b $\text{Goof} = [\sum [w(F_o^2 - F_c^2)] / (n - p)]^{1/2}$. ^c $\text{wR2} = [\sum [w(F_o^2 - F_c^2)] / \sum [w(F_o^2)]]^{1/2}$, where $w = 1/\sigma^2(F_o^2) + (aP)^2 + bP$, $P = (F_o^2 + 2F_c^2)/3$.

X-ray Crystallographic Data Collection and Refinement of the Structures. Black single crystals of **1**, **2**, **3**, an orange brown crystal of **1a**, and a deep red crystal of **2a** were coated with perfluoropolyether, picked up with a glass fiber, and mounted in the nitrogen cold stream of the diffractometers. Intensity data were collected at 100 K with use of graphite monochromated Mo K α radiation ($\lambda = 0.71073$ Å). Final cell constants were obtained from a least-squares fit of a subset of several thousand strong reflections. Data collection was performed by hemisphere runs taking frames at 0.3° (Siemens SMART) and 1.0° (Nonius Kappa-CCD) in ω . Crystal faces of **1a**, **2**, **2a**, and **3** were determined and the Gaussian absorption correction routine of XPREP⁹ was used to account for absorption effects. A semiempirical absorption correction using the program SADABS⁸ was performed on the data set of **1**. Crystallographic data of the compounds and diffractometer types used are listed in Table 1. The Siemens ShelXTL⁹ software package was used for solution, refinement, and artwork of the structure. Structures **1a** and **2a** were readily solved by direct methods and difference Fourier techniques whereas the other solutions were obtained by the Patterson method. All non-hydrogen atoms were refined anisotropically and hydrogen atoms were placed at calculated positions and refined as riding atoms with isotropic displacement parameters.

Physical Measurements. UV–vis, EPR, and infrared spectra (KBr disks) have been recorded with apparatus described in refs 1–5. Similarly, the electrochemical and the magnetochemical equipment have been described previously^{1–5} as have the programs used for the EPR simulations.

Calculations. Relativistic density functional calculations were carried out with the ADF program system version 2000.02.¹⁰ The geometries of the complexes were optimized in C_{2h} symmetry by using the BP86 functional^{11,12} in the spin-polarized scalar relativistic ZORA option.¹³ For the geometry optimizations the ZORA basis set IV was used for Pt, II for hydrogen, and III for the remaining

atoms. For the property calculations the large ZORA basis set V was used for Pt and basis set IV for all other atoms. The neutral complex was optimized in the triplet state. Magnetic coupling parameters were calculated according to the procedures of van Lenthe et al. for **g**-tensors¹⁴ and hyperfine couplings (hfc's¹⁵). This formalism allows for the calculation of the **g**-tensor and orbital correction to the hfc's in a spin-restricted formalism while the Fermi-contact term and orbital dipolar term are calculated in a spin-unrestricted formalism.

Results and Discussion

Synthesis and Characterization of Complexes. Dark blue crystals of [Pd(L^{AP}-H)(bpy)] (**1**) and dark green crystals of [Pt(L^{AP}-H)(bpy)] (**2**) were obtained in ~70% yield from the reaction of the ligand H[L^{AP}] and [M^{II}(bpy)Cl₂] (M = Pd, Pt) in equimolar amounts in dry acetonitrile and 2 equiv of the base sodium methoxide under anaerobic conditions at elevated temperatures. Both **1** and **2** are diamagnetic, mononuclear species.

The one-electron-oxidized forms [M^{II}(L^{ISQ})(bpy)]PF₆ (M = Pd (**1a**), Pt (**2a**)) were obtained in excellent yields from reaction mixtures of **1** and **2** and an equimolar amount of ferrocenium hexafluorophosphate as clean one-electron oxidant in dry CH₂Cl₂ at ambient temperature. Crystals of **1a** are dark brown and those of **2a** dark red. Magnetic susceptibility measurements of solid samples of **1a** and **2a** in the temperature range 4–300 K revealed a temperature-independent magnetic moment (50–300 K) of 1.8 μ_B , respectively. Thus, both complexes possess an $S = 1/2$ ground state.

Dark blue microcrystals of [Pt^{II}(L^{ISQ})₂] (**3**) have been obtained in moderate yields from the reaction mixture of PtCl₂, the ligand H[L^{AP}] (1:2), and 4 equiv of NEt₃ in CH₃CN solution in the presence of air at 20 °C. The analogous

(8) Sheldrick, G. M. Universität Göttingen, 1994.

(9) ShelXTL, V.5; Siemens Analytical X-ray Instruments, Inc., 1994.

(10) ADF, V 2000.02; Scientific Computing and Modeling NV; Vrije Universiteit, Theoretical Chemistry; Amsterdam, The Netherlands.

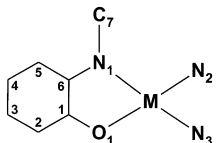
(11) Becke, A. D. *J. Chem. Phys.* **1988**, *84*, 4524.

(12) Perdew, J. P. *Phys. Rev. B* **1986**, *33*, 8822.

(13) van Lenthe, E.; Baerends, E. J.; Snijders, J. G. *J. Chem. Phys.* **1993**, *99*, 4597.

(14) van Lenthe, E.; Wormer, P. E. S.; van der Avoird, A. *J. Chem. Phys.* **1997**, *107*, 2488.

(15) van Lenthe, E.; van der Avoird, A.; Wormer, P. E. S. *J. Chem. Phys.* **1998**, *108*, 4783.

Table 2. Selected Bond Distances (Å) of Complexes


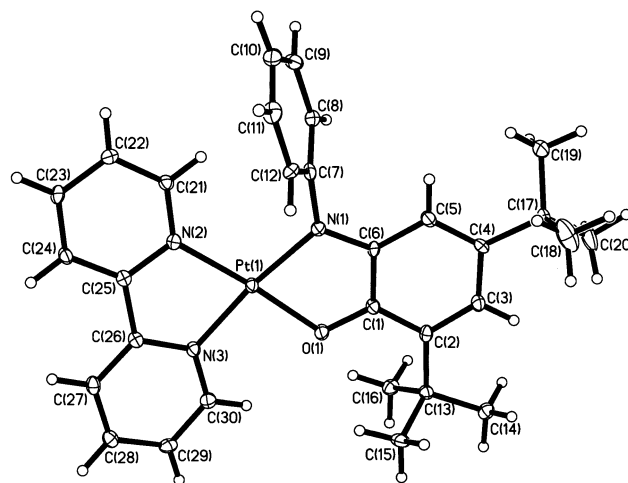
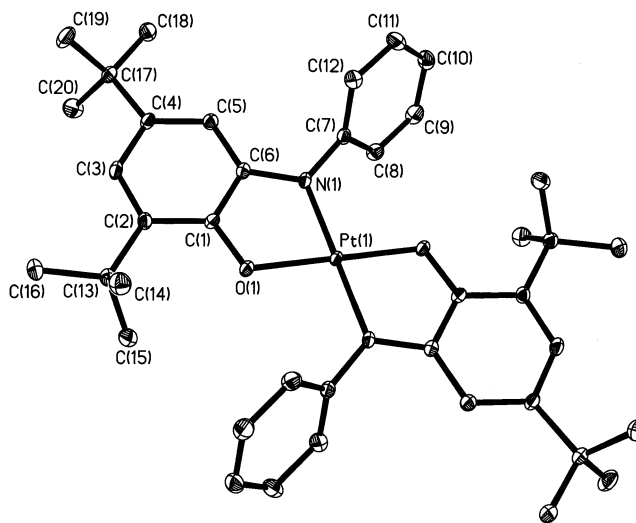
	1	2	1a	2a	3
M–N1	1.974(2)	1.985(3)	2.014(2)	2.011(4)	1.946(2)
M–N2	2.048(2)	2.015(3)	2.028(2)	2.028(4)	
M–N3	2.019(2)	1.997(3)	2.013(2)	2.011(3)	
M–O1	1.968(1)	1.980(2)	1.989(1)	1.996(3)	1.977(1)
N1–C7	1.410(2)	1.418(4)	1.433(2)	1.437(6)	1.429(3)
N1–C6	1.387(2)	1.390(4)	1.346(2)	1.350(5)	1.372(2)
C1–O1	1.348(2)	1.357(4)	1.309(2)	1.317(5)	1.317(2)
C1–C6	1.421(3)	1.417(4)	1.450(2)	1.429(6)	1.419(3)
C1–C2	1.406(2)	1.397(4)	1.428(3)	1.429(6)	1.427(3)
C2–C3	1.405(3)	1.404(5)	1.382(3)	1.394(6)	1.376(3)
C3–C4	1.398(3)	1.394(5)	1.437(2)	1.430(6)	1.430(3)
C4–C5	1.402(2)	1.405(4)	1.366(3)	1.376(6)	1.373(3)
C5–C6	1.395(2)	1.401(4)	1.420(3)	1.416(6)	1.414(3)

compounds $[M^{\text{II}}(\text{L}^{\text{ISQ}})_2]$ ($M = \text{Ni}, \text{Pd}$) have been described previously.² Complex **3** is diamagnetic ($S = 0$) as was judged from its “normal” ^1H NMR spectrum (see Experimental Section). It displays a typical very intense ($7.3 \times 10^4 \text{ M}^{-1} \text{ cm}^{-1}$) interligand charge-transfer band at 813 nm (see below and ref 2).

Crystal Structure Determinations. The crystal structures **1**, **1a**, **2**, **2a**, and **3** have been determined by high-quality X-ray crystallography at 100 K. Table 2 summarizes selected bond distances and Figure 1 shows the structure of the monocation in crystals of **2a**; the structures of the neutral molecules in **1** and **2** and that of the monocations in **1a** are very similar and not shown; they are available in the Supporting Information. Figure 2 shows the structure of the neutral molecules in crystals of **3**.

All complexes are square planar with an MN_3O donor set in **1**, **1a**, **2**, and **2a** and a PtN_2O_2 in **3**. In the following we compare the C–C, C–N, and C–O distances of the N,N- and N,O-coordinated bipyridine and aminophenolate derived ligands, respectively, in the neutral complexes **1** and **2** with the corresponding ones in the monocations of **1a** and **2a**. It is important to note that the average error of these bond lengths is small at $\pm 0.01 \text{ \AA}$ (3σ). It is therefore significant that the C–C distances in the bpy ligands and in the *N*-phenyl group of the aminophenolate ligands are equidistant within 0.01 \AA in all four structures. Thus the bpy and the *N*-phenyl groups are internal markers for the consistency of the structure determinations; they do not respond structurally upon one-electron oxidation of **1** (**2**) to **1a** (**2a**). In stark contrast, the C–O, C–N, and C–C distances of the *o*-aminophenol derived, O,N-coordinated ligands respond to this oxidation in a characteristic fashion. These distances are significantly different in **1** and **1a** and, similarly, in **2** and **2a**.

By using the data in Scheme 1 it is immediately possible to assign the protonation and oxidation levels of the aminophenol derived ligands as follows: For **1** and **2** it is clear that this ligand is dianionic ($\text{L}^{\text{AP-H}}\text{H}^{2-}$). The five C–C distances C1–C2, C2–C3, C3–C4, C4–C5, and C5–C6

**Figure 1.** Structure of the monocation $[\text{Pt}(\text{L}^{\text{ISQ}})(\text{bpy})]^+$ in crystals of **2a**. The structures of the neutral species $[\text{M}(\text{L}^{\text{AP-H}})(\text{bpy})]$ ($M = \text{Pd}$ (**1**), Pt (**2**)) and of the monocation in **1a** are very similar and are not shown (see Supporting Information). Small open circles represent H atoms.**Figure 2.** Structure of neutral complex $[\text{Pt}(\text{L}^{\text{ISQ}})_2]$ in crystals of **3**. H atoms omitted.

(Table 2) are within experimental error equidistant at $1.40 \pm 0.01 \text{ \AA}$; only C1–C6 is slightly longer at $1.42 \pm 0.01 \text{ \AA}$. The C–O bond at $1.35 \pm 0.01 \text{ \AA}$ is typical for a single bond of a phenolate group; the average C6–N1 distance is at $1.39 \pm 0.01 \text{ \AA}$ whereas the distance N1–C7 is at $1.41 \pm 0.01 \text{ \AA}$. The amido nitrogen N1 is sp^2 hybridized and not protonated. Thus **1** and **2** can safely be described as $[\text{M}^{\text{II}}(\text{L}^{\text{AP-H}})(\text{bpy})]$ ($M = \text{Pd}, \text{Pt}$).

The same distances in **1a** and **2a** clearly point to the presence of a monoanionic *o*-iminobenzosemiquinonato(1 $^-$) π -radical: average distances C2–C3 and C4–C5 are short at 1.38 ± 0.01 and $1.37 \pm 0.01 \text{ \AA}$, respectively, whereas all other C–C distances in this ring are rather long at $1.43 \pm 0.01 \text{ \AA}$. Thus this ring displays the characteristic features of a quinoid structure. At the same time, the C1–O1 distance at $1.315 \pm 0.01 \text{ \AA}$ and the C6–N1 distance at $1.35 \pm 0.01 \text{ \AA}$ are short indicating considerable double bond character. Thus **1a** and **2a** must be described as $[\text{M}^{\text{II}}(\text{L}^{\text{ISQ}})(\text{bpy})]^+$. Finally, in **3** there are clearly two of these ($\text{L}^{\text{ISQ}}\text{H}^{1-}$) radicals O,N-coordinated to the central Pt(II) ion: $[\text{Pt}^{\text{II}}(\text{L}^{\text{ISQ}})_2]$.

Table 3. Redox Potentials of Complexes^a

complex	$E^{1/2}$, V	$E^{2/2}$, V	$E^{3/2}$, V	$E^{4/2}$, V
1	0.352	-0.644	-1.890	
2	0.421	-0.585	-1.900	
3	0.70	0.20	-1.07	-1.64
[Pd(L ^{ISQ}) ₂] ^b	0.47	0.08	-0.99	-1.40
[Ni(L ^{ISQ}) ₂] ^b	0.042 ^c		-1.07	-1.64

^a Potentials are referenced vs the Fc⁺/Fc couple; CH₂Cl₂ solutions containing 0.10 M [N(*n*-Bu)₄]PF₆; glassy carbon working electrode; ferrocene internal standard. ^b Reference 2. ^c 2e process: [Ni^{II}(L^{ISQ})₂] → [Ni^{II}(L^{IBQ})₂]²⁺ + 2e; ref 2.

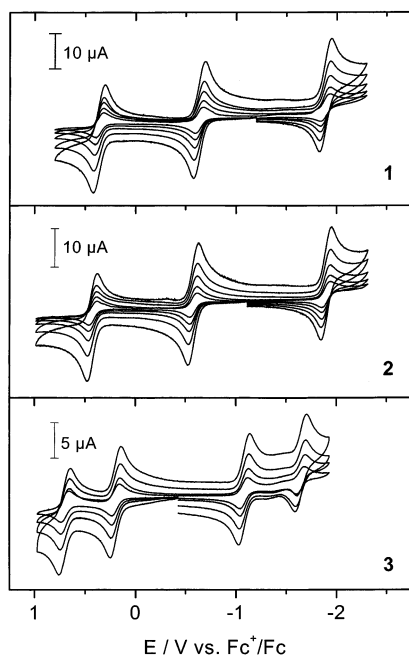
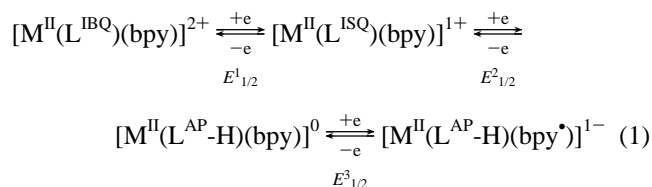


Figure 3. Cv of **1** (1×10^{-3} M), **2** (1.0×10^{-3} M), and **3** (0.4×10^{-3} M) in CH₂Cl₂ solution (0.10 M [N(*n*-Bu)₄]PF₆) at 20 °C (glassy carbon working electrode) at scan rates of 25, 50, 100, 200, and 400 mV s⁻¹ for **1** and **2** and 100, 200, 400, and 800 mV s⁻¹ for **3**.

Electro- and Spectroelectrochemistry. Cyclic voltammograms of all complexes have been recorded at 20 °C in CH₂Cl₂ solutions containing 0.10 M [N(*n*-Bu)₄]PF₆ as supporting electrolyte at a glassy carbon working electrode and a Ag/AgNO₃ reference electrode. Ferrocene was used as an internal standard, and potentials are referenced versus the ferrocenium/ferrocene couple (Fc⁺/Fc). Table 3 summarizes these results.

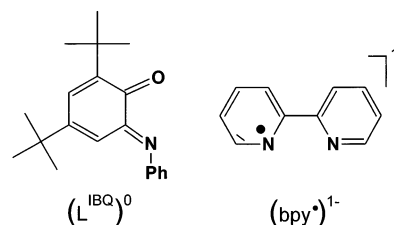
Figure 3 displays the cvs of **1**, **2**, and **3**. Both **1** and **2** show three reversible one-electron waves in the range +1.0 to -2.5 V, which correspond to the processes in eq 1 (M = Pd, Pt):



Interestingly, the redox potentials, $E^{1-3/2}$, are very similar for **1** and **2**; they do not vary greatly (60–70 mV) with a change of the second-row divalent Pd ion to the third-row

transition metal ion Pt. The cvs of **1a** and **2a** are identical with those shown in Figure 3 for **1** and **2**.

The one-electron oxidation of the monocations [M^{II}(L^{ISQ})(bpy)]¹⁺ to the dications [M^{II}(L^{IBQ})(bpy)]²⁺ (M = Pd, Pt) is a ligand-centered process where the *o*-iminobenzosemiquinonate anion is oxidized to the *o*-iminobenzoquinone, (L^{IBQ})⁰, as was judged from the changes observed in their electronic absorption spectra (see below). Similarly, the one-electron reduction of **1** and **2** is proposed to be a ligand-centered process where an N,N-coordinated 2,2'-bipyridine ligand is reversibly reduced to its monoanionic radical (bpy[•])¹⁻.^{16–19} Thus the species [M^{II}(L^{AP-H})(bpy[•])]¹⁻ (M = Pd, Pt) are proposed to be generated. They are not stable in solution at ambient temperature and, therefore, have not been characterized further.



The cv of **3** (Figure 3, bottom) is very similar to those reported for [Cu^{II}(L^{ISQ})₂] and [Pd(L^{ISQ})₂].² In all of these cases, four reversible one-electron-transfer waves are observed of which two correspond to successive one-electron reductions and two to successive one-electron oxidations. This electrochemical behavior is typical for this class of square-planar complexes containing two *o*-phenylenediamido and related ligands.²⁰ Since the redox potentials $E^{1-4/2}$ for all three complexes are very similar irrespective of the nature of the central metal ion (Cu^{II}, Pd^{II}, Pt^{II}), we assign these processes as ligand centered, eq 2.

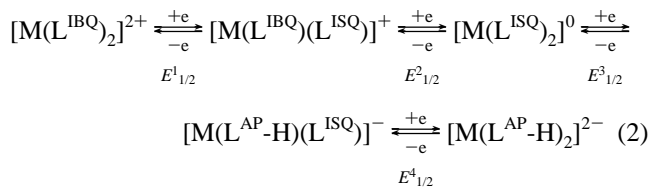


Figure 4 shows the electronic spectra in the visible of **1** (top) and **2** (bottom) and of their respective mono- and dications which were generated by controlled potential electrolysis in CH₂Cl₂ solutions containing 0.10 M [N(*n*-Bu)₄]PF₆. Table 4 summarizes the electronic spectra. In the

- (16) Tokel-Takvoryan, N. E.; Hemingway, R. E.; Bard, A. J. *J. Am. Chem. Soc.* **1973**, *95*, 6582.
 (17) McInnes, E. J. L.; Welch, A. J.; Yellowlees, L. J. *Chem. Commun.* **1996**, 2393.
 (18) McInnes, E. J. L.; Farley, R. D.; Macgregor, S. A.; Taylor, K. J.; Yellowlees, L. J.; Rowlands, C. C. *J. Chem. Soc., Faraday Trans.* **1998**, *94*, 2985.
 (19) McInnes, E. J. L.; Farley, R. D.; Rowlands, C. C.; Welch, A. J.; Yellowlees, L. J. *J. Chem. Soc., Dalton Trans.* **1999**, 4203.
 (20) (a) Balch, A. L.; Holm, R. H. *J. Am. Chem. Soc.* **1966**, *88*, 5201. (b) Holm, R. H.; Balch, A. L.; Davison, A.; Muki, A.; Berry, T. *J. Am. Chem. Soc.* **1967**, *89*, 2866. (c) Forbes, C. E.; Gold, A.; Holm, R. H. *Inorg. Chem.* **1971**, *10*, 2479. (d) Stiefel, E. I.; Waters, J. H.; Billig, E.; Gray, H. B. *J. Am. Chem. Soc.* **1965**, *87*, 3016.

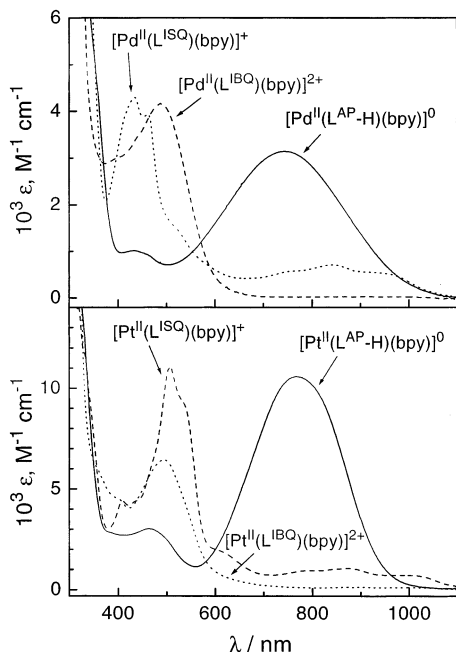
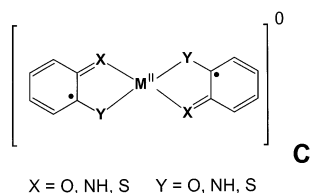


Figure 4. Electronic spectra of **1** (top) and **2** (bottom) and their respective mono- and dications in CH_2Cl_2 solutions (0.10 M $[\text{N}(n\text{-Bu})_4]\text{PF}_6$). The mono- and dications were generated from **1** or **2** by controlled potential coulometry.

visible, the very intense absorption bands at 745 nm ($\epsilon = 3.2 \times 10^3 \text{ L mol}^{-1} \text{ cm}^{-1}$) for **1** and at 780 nm ($\epsilon = 1.05 \times 10^4 \text{ L mol}^{-1} \text{ cm}^{-1}$) for **2**, as well as the absorption maximum at 813 nm ($\epsilon = 7.3 \times 10^4 \text{ L mol}^{-1} \text{ cm}^{-1}$) for **3** (see below), are due to a spin- and dipole-allowed charge-transfer transition between the two bidentate ligands in square-planar complexes (Scheme 3).²¹ These transitions have been observed in all complexes of the type C; they are nearly independent of the nature of the central metal ion (Co^{II} , Ni^{II} , Cu^{II} , Pd^{II} , Pt^{II}) as discussed in ref 2.



The electronic spectra of **1a** and **2a** allow the characterization of a single O,N-coordinated $(\text{L}^{\text{ISQ}})^{1-}$ radical. As shown before by us for $[\text{Cu}^{\text{II}}(\text{dmtacn})(\text{L}^{\text{ISQ}})]\text{PF}_6$ where dmtacn is the spectroscopically innocent amine 1,4-dimethyl-1,4,7-triazacyclononane, this π -radical ligand displays four bands in the visible $> 500 \text{ nm}$ (510, 730, 820, 980 nm) with molar extinction coefficients $(0.6\text{--}1.5) \times 10^3 \text{ L mol}^{-1} \text{ cm}^{-1}$.² In contrast, the spectra of the dications containing an O,N-coordinated quinone, (L^{IBQ}) , display no absorptions $> 600 \text{ nm}$ but two strong bands at 400 and 495 nm, which can be assigned to quinone CT bands since the uncoordinated quinone in CH_2Cl_2 solution displays two such absorption maxima at 396 ($\epsilon = 4.8 \times 10^3 \text{ M}^{-1} \text{ cm}^{-1}$) and 488 nm ($\epsilon = 2.7 \times 10^3 \text{ M}^{-1} \text{ cm}^{-1}$).² Interestingly, the spectrum of

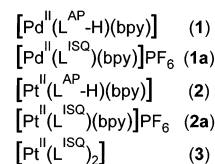
Table 4. Electronic Spectra of Complexes^a

	λ_{max} , nm ($10^3 \epsilon$, $\text{L mol}^{-1} \text{ cm}^{-1}$)
$[\text{Pd}(\text{L}^{\text{AP-H}})(\text{bpy})]$	450 (1.0), 745 (3.2)
$*[\text{Pd}(\text{L}^{\text{ISQ}})(\text{bpy})]^+$	425 (4.25), 470 (3.9), 510 sh (1.5), 730 sh (0.6), 820 (0.7), 980 sh (0.6)
$*[\text{Pd}(\text{L}^{\text{IBQ}})(\text{bpy})]^{2+}$	400 sh (3.0), 495 (4.2)
$[\text{Pt}(\text{L}^{\text{AP-H}})(\text{bpy})]$	480 (3.0), 780 (10.5)
$*[\text{Pt}(\text{L}^{\text{ISQ}})(\text{bpy})]^+$	503 (11.0), 535 sh (9.1), 610 sh (2.0), 780 sh (1.0), 880 sh (1.2), 1000 sh (0.8)
$*[\text{Pt}(\text{L}^{\text{IBQ}})(\text{bpy})]^{2+}$	400sh (4.5), 495 (6.3)
$*[\text{Pt}(\text{L}^{\text{IBQ}})_2]^{2+}$	427 (33.2), 507 (19.5)
$*[\text{Pt}(\text{L}^{\text{ISQ}})(\text{L}^{\text{IBQ}})]^+$	298 (15.0), 488 (15.4), 531 (17.3), 622 (15.1), 681 (21.5)
$[\text{Pt}(\text{L}^{\text{ISQ}})_2]$	224 (60), 318 (13), 430 (5.3), 628 (7.3), 813 (73)
$*[\text{Pt}(\text{L}^{\text{AP-H}})(\text{L}^{\text{ISQ}})]^-$	305 (15.5), 339 (15.4), 363 (15.5), 577 (3.4), 821 (3.9), 1059 (15.7)
$*[\text{Pt}(\text{L}^{\text{AP-H}})_2]^{2-}$	346 (21.1), 576 (2.2)

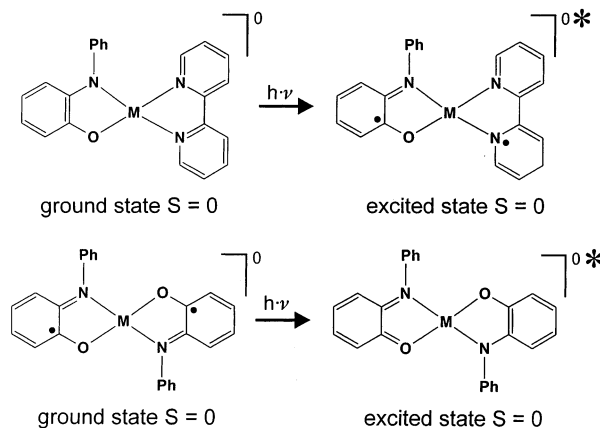
^a In CH_2Cl_2 solution; species marked with an asterisk were electrochemically generated in CH_2Cl_2 solution containing 0.10 M $[\text{N}(n\text{-Bu})_4]\text{PF}_6$.
^b These spectra are identical with those of CH_2Cl_2 solutions of $[\text{M}(\text{L}^{\text{ISQ}})(\text{bpy})]\text{PF}_6$ (M = Pd (**1a**), Pt (**2a**)).

Scheme 2. Complexes and Labels

Complexes:



Scheme 3. Interligand CT Transitions of **1**, **2**, and **3**



$[\text{Cu}(\text{dmtacn})(\text{L}^{\text{AP-H}})]^0$ containing the O,N-coordinated dianion $(\text{L}^{\text{AP-H}})^{2-}$ is featureless at $> 400 \text{ nm}$. Note that no interligand CT band as in **1** and **2** is observed because dmtacn is a very poor π -acceptor ligand. Thus, it is clear that the oxidation levels of O,N-coordinated *o*-aminophenolate derivatives can be established from their electronic spectra.

Figure 5 shows the electronic spectra of **3**, and of its two reduced and two oxidized forms, respectively, which were generated by controlled-potential electrolysis of CH_2Cl_2 solutions of **3** (millimolar) containing 0.10 M $[\text{N}(n\text{-Bu})_4]\text{PF}_6$ as supporting electrolyte at $-20 \text{ }^\circ\text{C}$. The potential for the generation of the monocation was fixed at 0.4 V, whereas that for the monoanion was fixed at -1.4 V . Both the oxidation and the reduction went smoothly and in each case one electron per Pt ion was either removed or added ($n = \pm 1.0 \pm 0.05 \text{ e/Pt}$). The same holds for the dication and

(21) Vogler, A.; Kunkely, H. *Comments Inorg. Chem.* **1990**, *9*, 201.

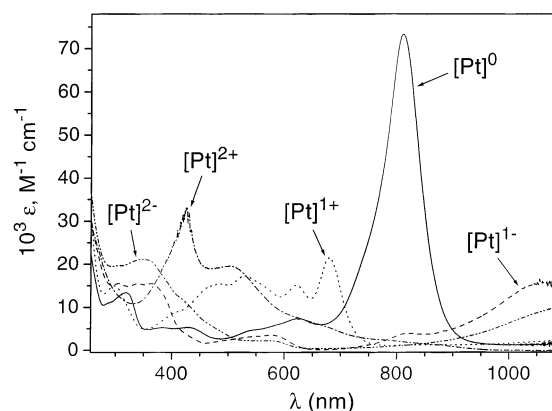


Figure 5. Electronic spectra of **3** and of its mono- and dication, and of its mono- and dianion. The oxidized and reduced forms of **3** were generated electrochemically at $-20\text{ }^\circ\text{C}$ in CH_2Cl_2 solution (0.10 M $[\text{N}(n\text{-Bu})_4]\text{PF}_6$).

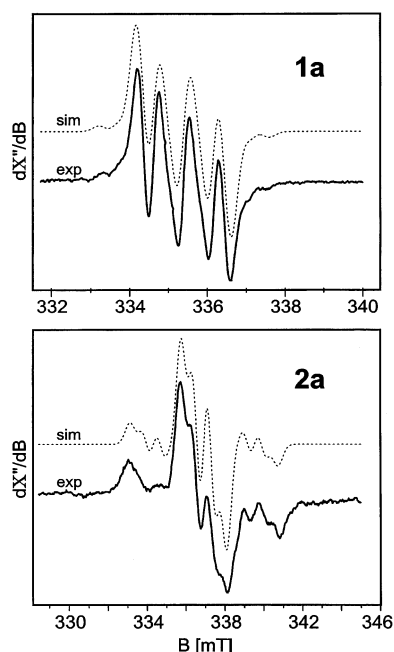


Figure 6. X-band EPR spectra of **1a** (top) and **2a** (bottom) in CH_2Cl_2 solution at 298 K (frequency 9.4555 Hz; modulation 0.4 G; power 10 mW) and simulation with parameters given in the text.

dianion which were electrochemically generated from the monocation and monoanion. To check the chemical integrity of the thus generated cations and/or anions, cyclic voltammograms were recorded immediately after the corresponding electrolysis experiment had been performed. In all cases a cv as shown in Figure 3 (bottom) for **3** was obtained. The spectra shown in Figure 5 are very similar to those reported previously for the two oxidized and two reduced forms of $[\text{Ni}^{\text{II}}(\text{L}^{\text{ISQ}})_2]$ and $[\text{Pd}^{\text{II}}(\text{L}^{\text{ISQ}})_2]$.² Thus ligand oxidation levels as in eq 2 can be readily assigned.

X-Band EPR Spectroscopy. The X-band EPR spectra of CH_2Cl_2 solutions of **1a** and **2a** have been recorded at 298 K and are shown in Figure 6. Both spectra display a hyperfine split $S = 1/2$ signal at $g_{\text{iso}} = 2.002$ for **1a** and $g_{\text{iso}} = 2.0$ for **2a** in agreement with the notion that both complexes contain an O,N-coordinated *o*-iminobenzosemiquinonato radical. Satisfactory simulations were obtained by using the following parameters: for the spectrum of **1a**, $a(^{14}\text{N}) = 7.71\text{ G}$ (21.6

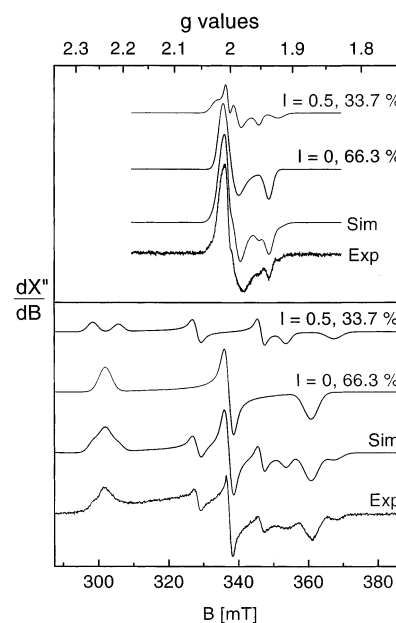


Figure 7. X-band EPR spectra of the electrochemically generated monocation $[\text{Pt}(\text{L}^{\text{IBQ}})(\text{L}^{\text{ISQ}})]^+$ (top) and monoanion $[\text{Pt}(\text{L}^{\text{ISQ}})(\text{L}^{\text{AP-H}})]^-$ (bottom) in CH_2Cl_2 (0.10 M $[\text{N}(n\text{-Bu})_4]\text{PF}_6$) at 50 and 10 K, respectively. Conditions: frequency 9.45684 and 9.45478 GHz; power 50.7 and 10 μW ; modulation 12 G for both spectra. Simulation parameters for the monocation: $g_x = 1.937$, $g_y = 1.997$, $g_z = 2.012$; $a(^{195}\text{Pt}, I = 0.5, 33.7\%)$: (55, 25, 42) G; and for the monoanion: $g_x = 1.873$, $g_y = 2.001$, $g_z = 2.234$; $a(^{195}\text{Pt}, I = 0.5, 33.7\%)$ = 134, 187, 88 G.

MHz); $a(^1\text{H}) = 4.6\text{ G}$ (12.9 MHz), $a(^{105}\text{Pd}, I = 2.5, 22.2\%) = 3.56\text{ G}$ (10.0 MHz) (line width 2.3 G); and for the spectrum of **2a**, $a(^{14}\text{N}) = 7.1\text{ G}$ (19.9 MHz); $a(^1\text{H}) = 4.67\text{ G}$ (13.3 MHz), $a(^{195}\text{Pt}, I = 0.5, 33.7\%) = 50.7\text{ G}$ (142.0 MHz) (line width: 3.4 G). These data clearly show the semiquinone character of the ligand $(\text{L}^{\text{ISQ}})^{\cdot-}$.

Similarly, the one-electron-oxidized form of **3** is a paramagnetic $S = 1/2$ species as is its one-electron-reduced form. The X-band EPR spectra are shown in Figure 7. From a simulation of the spectrum of the monocation three g -values 1.937, 1.997, 2.012 and a ^{195}Pt hyperfine splitting of $a_{\text{iso}}(^{195}\text{Pt}) = 41\text{ G}$ (111–115 MHz) are calculated. This spectrum indicates the presence of the radical species $[\text{Pt}^{\text{II}}(\text{L}^{\text{ISQ}})(\text{L}^{\text{IBQ}})]^+$. Interestingly, the aminothiophenolato derivative $[\text{Pt}^{\text{II}}(\text{L}_S\text{IBQ})(\text{L}_S\text{ISQ})]^+$ displays a similar EPR spectrum at 10 K ($g = 1.998, 2.015, 2.009$) with $a(^{195}\text{Pt}) = 9.5\text{ G}$ (~ 26.6 MHz), where $\text{H}[\text{L}_S\text{AP}]$ is 2,4-di-*tert*-butyl-6-aminothiophenol and $(\text{L}_S\text{ISQ})^{\cdot-}$ and (L_SIBQ) are the corresponding oxidized ligand derivatives.⁶

The spectrum of the monoanion $[\text{Pt}^{\text{II}}(\text{L}^{\text{ISQ}})(\text{L}^{\text{AP-H}})]^-$ displays $g_z > g_{x,y}$ ($g_x = 1.873$, $g_y = 2.001$, $g_z = 2.234$) and large hfc 's $A(^{195}\text{Pt}) = 134, 187, \text{ and } 88\text{ G}$ (351, 523, and 275 MHz). We conclude that the unpaired electron must possess considerable metal d orbital character. Again, this spectrum is very similar to that reported for $[\text{Pt}^{\text{II}}(\text{L}_S\text{ISQ})(\text{L}_S\text{AP-H})]^-$, which displays the expected $S = 1/2$ signal in its X-band EPR spectrum with $g_x = 1.827$, $g_y = 2.031$, $g_z = 2.205$ and a large hyperfine splitting of $a_{\text{iso}}(^{195}\text{Pt}) = 109\text{ G}$ (~ 309 MHz).⁶

All square-planar cationic complexes of the type $[\text{M}^{\text{II}}(\text{L}^{\text{IBQ}})(\text{L}^{\text{ISQ}})]^+$ (where $\text{M}^{\text{II}} = \text{Ni}^{\text{II}}, \text{Pd}^{\text{II}}, \text{Pt}^{\text{II}}$; and $\text{L}^{\text{IBQ}} =$

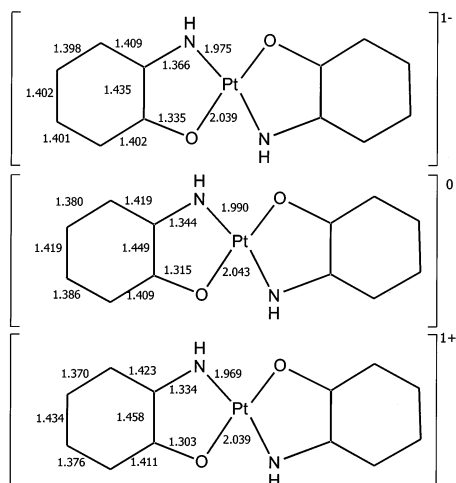


Figure 8. Calculated structures (BP86 functional, spin-polarized, scalar relativistic ZORA formalism) of **3** and of its monocation and monoanion, respectively. Bond distances are given in Å.

o-benzoquinone ligand, and $(L^{ISQ})^-$ is its *o*-benzosemiquinonato π -radical) display X-band EPR signals at $g \sim 2.0$ with very small g anisotropy whereas, in stark contrast, the corresponding monoanions $[Pt^{II}(L^{AP-H})(L^{ISQ})]^-$ display rhombic EPR signals with a rather large g anisotropy. This different spectroscopic behavior has been noted and discussed in the past,²⁰ but no consistent interpretation has been given.

Density Functional Calculations. For heavy transition metal containing molecules such as Pt it is necessary to resort to a treatment that explicitly includes relativistic effects. In this study this was accomplished by using the scalar relativistic ZORA method of van Lenthe and co-workers¹³ for the geometry optimizations and a spin-orbit corrected, spin-restricted formalism for the property calculations.^{14,15}

The calculated structures for **3** together with its anion and its cation are shown in Figure 8. In these calculations the neutral complex has been calculated in the triplet state in accord with the proposal that it is best described as a diradical.^{2,6} The structures of the triplet and singlet states should be rather similar and the triplet state is computationally more readily accessible. The comparison with the experimental data (Table 2) reveals that the spin-polarized ZORA calculations overestimate the metal–ligand bond lengths by ~ 0.05 Å. This is not a feature of the relativistic treatment but of the BP86 functional used. The bond lengths within the ring are reproduced with much better accuracy and agree with experiment to ~ 0.01 Å. Again this is typical of the BP86 functional. Thus, the calculations support the idea that the neutral complex **3** does in fact contain two coordinated radicals. The one-electron-oxidized form shows a slightly more pronounced distortion toward a quinoidal structure and also slightly reduced metal–ligand bond lengths. By contrast, the anionic form shows a less pronounced distortion than the neutral complex. Both results are consistent with a ligand-centered oxidation or reduction that brings the rings closer to their quinone form in the case of the cation and closer to the aromatic form in the case of the anion.

Table 5. Calculated (Spin–Orbit Corrected ZORA) and Experimental Values (in parentheses) for the g -Tensors of the Monocation and Monoanion of **3**

	g_1	g_2	g_3
$[Pt^{II}(L^{ISQ})(L^{IBQ})]^+$	1.999 (2.012)	1.996 (1.997)	1.988 (1.937)
$[Pt^{II}(L^{ISQ})(L^{AP-H})]^-$	2.269(y) ^a (2.234)	1.971(x) ^a (2.001)	1.801(z) ^a (1.873)

^a Calculated g -tensor orientation.

Table 6. Calculated and Experimental Values (in parentheses) for ^{195}Pt Hyperfine Couplings of the Monocation and Monoanion of **3**

	A_1 , MHz	A_2 , MHz	A_3 , MHz
$[Pt^{II}(L^{ISQ})(L^{IBQ})]^+$	−104 ($ a_{\text{iso}} = 110$)	−65	−27
$[Pt^{II}(L^{ISQ})(L^{AP-H})]^-$	−510(y) ^c +343(y) ^c (1275 g_{max})	−176(x) ^c −93(x) ^c (1523 g_{mid})	−185(z) ^{a,c} +185(z) ^{b,c} (1351 g_{min})

^a Spin-polarized scalar relativistic ZORA. ^b Spin-restricted spin-orbit corrected ZORA. ^c Calculated orientation.

Table 5 compares the calculated EPR g -values with the experimentally derived parameters. The calculations faithfully reproduce the experimental finding that the cation has a g -tensor that resembles an organic radical while the anion has a much more anisotropic g -tensor. For the anion the calculated orientation of the g -tensor is such that the largest component is in the (x,y) plane and perpendicular to the long axis of the complex (taken as the x -axis). The g_{mid} component is also in the (x,y) plane and points along x while the smallest component is along the normal of the complex plane.

The calculated ^{195}Pt hfc's are presented in Table 6. Unfortunately, the present stage of development of the ZORA method does not allow the simultaneous inclusion of spin-orbit coupling and spin-polarization in the calculation of the ^{195}Pt hyperfine tensor. However, since the second-order spin-orbit contribution to the hyperfine coupling is essentially proportional to the deviation of the g -values from the free-electron value,²⁰ it is readily appreciated that the second-order correction should be negligible for the cation where the g -shifts are extremely small. The calculated maximal hfc for the cation of magnitude 104 MHz agrees well with the experimentally deduced coupling constant with a magnitude of ~ 110 MHz, but the anisotropy could not be determined from experiment due to the small anisotropy in the g -tensor. For the anion, the spin-orbit corrected and scalar relativistic ZORA results are very different, which indicates a large second-order spin-orbit contribution to the ^{195}Pt hfc. The ADF program currently does not allow for a combined calculation that allows for the simultaneous inclusion of all important effects for hfc calculations (i.e. spin-polarization and spin-orbit coupling). Agreement with the experimental numbers can therefore not be expected for the monoanion. However, qualitatively, spin-orbit coupling strongly counteracts the strongly negative ^{195}Pt hfc in the direction of g_{max} , which is in agreement with the experimental finding that the smallest component of the ^{195}Pt hfc is oriented along this direction. This leaves the larger components of the ^{195}Pt hfc to the g_{mid} components which have a positive contribution from the spin-dipolar interaction.

In summary, while the results of the EPR experiments would seem to argue for a metal-centered reduction due to

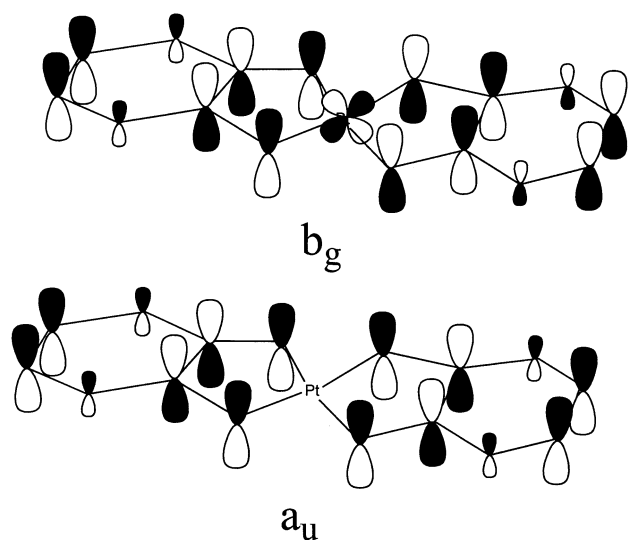


Figure 9. The two redox-active MOs of **3**. The a_u MO is lower in energy and the SOMO in the monocation of **3**, whereas the b_g MO is higher in energy and the SOMO in the monoanion of **3**.

the large g -shifts and ^{195}Pt hfc and a ligand-centered oxidation due to the small g -shifts and small ^{195}Pt hfc, the interpretation of this result is more complex.

The calculated magnetic parameters can be understood in terms of a simple model that only involves two molecular orbitals which are depicted in Figure 9. These two MOs are basically the symmetric and antisymmetric combination of the SOMO of the free semiquinonate ligand.

According to our calculations the ground state of the monocation is 2A_u with the a_u MO in Figure 9 being singly occupied. Since this MO transforms “ungerade” under inversion it cannot mix with any metal orbital. Consequently, a large ^{195}Pt hfc cannot be expected and is also not observed experimentally. The residual ^{195}Pt hfc is consequently attributed to spin polarization effects which appear to be reasonably well modeled by the spin-unrestricted ZORA calculations presented in the previous paragraph. In addition, the lack of metal character in the SOMO makes the spin-orbit coupling of excited states with the ground state very inefficient. Consequently, there is very little angular momentum in the ground-state wave function and the observed and calculated g -shifts are very small and reflect the radical character of the ground state.

For the monoanion the situation is exactly reversed. Since the orbital transforms “gerade” under inversion it readily mixes with the out-of-plane d_{xz} orbital of the Pt(II) and thereby acquires some metal character. This metal character gives rise to a sizable first-order ^{195}Pt hyperfine coupling observed experimentally and also enhances the spin-polarization of the Pt-core that is responsible for the isotropic Fermi contact contribution to the hfc. Since the ground-state 2B_g readily mixes with relatively low-lying d–d excited states it also has a sizable orbital angular momentum that manifests itself in the large g -shifts observed experimentally. The calculated value for the spin density at the central Pt is 23.7%, which appears to be a reasonable estimate.^{17–19}

Conclusions. The most salient feature of the present study is the unequivocal identification of an O,N-coordinated

o-iminobenzosemiquinonate(1[−]) π -radical in the cations $[\text{M}^{\text{II}}(\text{L}^{\text{ISQ}})(\text{bpy})]^+$ ($\text{M} = \text{Pd}, \text{Pt}$) and the neutral species $[\text{Pt}^{\text{II}}(\text{L}^{\text{ISQ}})_2]$ by X-ray crystallography. In contrast, for the corresponding neutral species $[\text{M}^{\text{II}}(\text{L}^{\text{AP-H}})(\text{bpy})]$ X-ray crystallography confirms the presence of an O,N-coordinated, closed shell *o*-amidphenolato(2[−]) dianion.

The combination of EPR experiments and relativistic DFT calculations has given insight into the electronic structures for the monocation and monoanion of **3**. Thus, the monocation features a delocalized mixed-valence system where the unpaired electron is evenly shared by the two noninnocent ligands. There is no metal character in the delocalized SOMO because it transforms in an “ungerade” irreducible representation and no d-orbital is of appropriate symmetry for mixing with it. Consequently, the whole radical character resides on the ligands which are bound to a spectroscopically innocent Pt(II) ion. Each of the ligands has, on average, one-half electron in excess of its quinone form, which explains the more pronounced ring distortion relative to the neutral complex which features two semiquinonates bound to a central Pt(II). The situation for the monoanion is different. The monoanion can also be regarded as a delocalized mixed-valence system where, again, the unpaired electron is mainly located on the ligands that are, on average, one-half electron short of an aromatic configuration. Consequently, the ring distortion is much less pronounced than in either the neutral complex or the monocation. An important difference from the monocation is that in the monoanion the delocalized SOMO transforms in a “gerade” irreducible representation. Thus, it can acquire some metal d-character. This mixing of the SOMO with the metal d-orbitals is to be interpreted as back-bonding of a Pt(II) ion to the π -accepting ligands and *not* as Pt(I) character. The metal character in the SOMO gives rise to much larger ^{195}Pt hfc because here the mechanism that gives rise to hyperfine coupling of the unpaired electron with ^{195}Pt is “direct” while in the monocation it is entirely indirect and due to spin-polarization. In addition, the “gerade” symmetry of the ground state in the monoanion allows the ground state to effectively spin-orbit couple with the d–d excited states (note that even in the presence of spin-orbit coupling parity is a good quantum number). This introduces significant orbital angular momentum in the ground state, which is evident in both the experiment and the calculation as a significant deviation of the g -tensor components from the free-electron g -value.

Acknowledgment. We thank the Fonds der Chemischen Industrie for financial support. X.S. is grateful to the Max-Planck Society for a stipend and H.C. thanks the Alexander von Humboldt Foundation for a postdoctoral fellowship.

Supporting Information Available: Figure S1–S3 displaying the structures of complexes in **1**, **1a**, and **2** and tables of crystallographic structure refinement data, atom coordinates, bond lengths and angles, anisotropic thermal parameters, and calculated positional parameters of H atoms for complexes **1**, **1a**, **2**, **2a**, **3**. This material is available free of charge via the Internet at <http://pubs.acs.org>.

IC011297K